QUANTUM INFORMATION PROCESSING USING NUCLEAR AND ELECTRON MAGNETIC RESONANCE : REVIEW AND PROSPECTS

BY J. BAUGH, J. CHAMILLIARD, C.M. CHANDRASHEKAR, M. DITTY, A. HUBBARD, R. LAFLAMME, M. LAFOREST, O. MOUSSA, C. NEGREVERGNE, M. SILVA, S. SIMMONS, C.A. RYAN, D.G. CORY, J.S. HODGES, AND C. RAMANATHAN

Quantum information processing is changing our fundamental understanding of what information is and how it can be manipulated. Recent work has lead to experimental proof-of-principle demonstrations of the control of small quantum systems, and new devices capable of harnessing larger quantum systems could change the technological landscape of the 21st century. There exist many proposals to physically realize such a quantum processor and presently a few of these models are able to manipulate quantum bits (qubits): quantum systems whose observables are given by the Pauli matrices. A qubit encodes a fundamental unit of quantum information. One such proposal uses the nuclear and electron magnetic moments and is the subject of this short review.

Many atoms' nuclei possess a magnetic moment. When placed in an external magnetic field, these moments result in discrete energy level systems that can be manipulated with resonant electromagnetic radiation leading to nuclear magnetic resonance (NMR). It was first observed more than half a century ago by Purcell and Bloch [1,2]. It has become a powerful analytical tool with many applications such as non-destructively determining molecular structures for chemistry as well as static and dynamic imaging in both industry and medicine.

Many nuclei such as ^1H or ^{13}C are spin-1/2 quantum system. These are ideal qubits. The initial state of the system is obtained by allowing it to thermalize. By irradiating these nuclei at the appropriate frequency it is possible to rotate their individual states one at a time leading to the so called single-qubit gates. Nuclei affect each other through interactions that can also be controlled, leading to two-qubit gates. By composing these two sets of gates we can reach any unitary transformation. This is known as universality [3]. After an algorithm consisting of a series of these gates, the final state can be observed by measuring the current induced by the rotating magnetic moments of the sample in a conducting coil. Algorithms are to be performed on a timescale shorter than the characteristic decoherence time of the system, which is about 100 times the gate time in liquid state NMR.

The strength of NMR technology is the exquisite control that can be implemented in multi-qubit systems. Many decades of radio-frequency (RF) engineering improvements today provide sufficient control to implement experimental benchmarks such as quantum error correcting codes and simulations of quantum physics systems, among many others. In this paper, we first give a brief review of both liquid and solid state NMR and then discuss recent work using both electron and nuclear spins to form more powerful information processing devices. The latter work provides a pathway to reach high purity states which has been a weakness of the liquid state NMR proposal.

The rest of the paper is organized as follows: the first five sub-sections under Liquid State NMR give a detailed introduction to the concepts of NMR based quantum information processing in the liquid state environment; the next two sub-sections introduce more advanced ideas of quantum control based on refocusing and optimal control methods; the second section (Solid State NMR) describes the solid state environment, a three-qubit solid state processor and experimental results demonstrating high-fidelity control; the third section (Control of Coupled Electron-Nuclear Systems) discusses a new direction involving systems of coupled electron and nuclear spins, including motivations, prospects, and recent progress; and finally the last section concludes the paper.

SUMMARY

Quantum information is an exciting field promising a revolution in information processing. A key ingredient for the advancement of this field is the development of technologies that can implement quantum information processing (QIP) tasks. This paper describes recent progress using nuclear magnetic resonance (NMR) as the platform. The basic ideas of NMR quantum information processing are detailed, examining the successes and limitations of liquid and solid state experiments. Finally, a future direction for implementing quantum processors is suggested, utilizing both nuclear and electron spin degrees of freedom.

J. Baugh, J. Chamilliard, C.M. Chandrashekar, M. Ditty, A. Hubbard, R. Laflamme <laflamme@iqc.ca>, M. Laforest, O. Moussa, C. Negrevergne, M. Silva, S. Simmons, and C.A. Ryan, Institute for Quantum Computing, University of Waterloo, Waterloo, ON, N2L 3G1 and D.G. Cory, J.S. Hodges, and C. Ramanathan, Dept. of Nuclear Science and Engineering, Massachusetts Institute of Technology, 77 Massachusetts Ave., Cambridge, MA 02130

LIQUID STATE NMR

Magnetic interactions

In the semi-classical picture, the spin of a nucleus behaves like the dipolar moment of a magnet possessing angular momentum parallel to its magnetic moment. When placed in a constant magnetic field pointing along a certain direction, (customarily defined as the z direction) the dipolar moment precesses around this axis. The frequency of this precession is called the Larmor frequency and is dependent on the external magnetic field, the nuclear isotope and its chemical environment within the molecule. For quantum information purposes, we are mainly interested in spin-1/2 nuclei (e.g. ^1H, ^{13}C, ^{15}N, ^{19}F, ^{29}Si and ^{31}P to name a few).

Placed in magnetic fields generated by modern superconducting magnets, different species of nuclei have differences in Larmor frequency on the order of MHz. For example, the Larmor frequency of ^1H is about 500 MHz in a 11.7 Tesla magnet, while that of ^{13}C is about 125 MHz. Depending on the symmetry of the molecule, two nuclei of the same species can either have the same Larmor frequency, or can have a frequency difference (called chemical shift) ranging from a few Hz to several kHz. Typical liquid state NMR experiments involve an ensemble of around 10^{20} identical molecules dissolved in a solvent whose effect on the nuclear magnetic moments of our molecules can be neglected.

When two spins are spatially close, their dipolar moments interact with each other. The strength of this coupling is dependent on the distance between the two spins and their relative orientation with respect to the external magnetic field. In a liquid, the molecules move and rotate around each other on a much shorter time scale than the interactions occurring between them. This causes the intermolecular and intra-molecular dipolar interactions to average to zero on the NMR time scale (i.e. the Larmor period time scale). In solid state NMR, however, dipolar interactions remain and can be controlled as discussed in the second section (Solid State NMR).

Within the same molecule, there are still interactions between the spins in the liquid state. If the wavefunctions of bonding electrons overlap spatially with a pair of nuclear spins, the electron mediates an effective interaction between the nuclear spins. This interaction is independent of the external magnetic field and the orientation of the molecule, which inspires its name: scalar coupling (also called indirect spin-spin coupling, or J-coupling).

The NMR Hamiltonian

As mentioned above, in liquid state NMR the intermolecular spin interactions are suppressed. This causes the molecules to be effectively isolated from each other, and therefore a description of the spin dynamics of an ensemble of molecules is well approximated by the spin dynamics of a single molecule. If we consider a molecule containing N spin-1/2 nuclei, then the nat-

ural Hamiltonian of this system in a large homogeneous magnetic field $\vec{B}_0$ pointing in the z direction is given by

$$H_{nat} = \frac{1}{2}\sum_{i=1}^{N} 2\pi v_i^L \sigma_z^i + \frac{\pi}{2}\sum_{i<j} J_{ij}\sigma_z^i\sigma_z^j \tag{1}$$

where $v_i^L = \omega_i^L/2\pi = \gamma_i|\vec{B}_0|$ is the Larmor frequency of the ith nucleus with gyromagnetic ratio γ_i, J_{ij} is the coupling strength between nucleus i and j and σ_z^i is the z Pauli matrix of the ith spin.

The first term in the Hamiltonian describes the precession of the spins due to their coupling to the external magnetic field, while the second term describes the J-coupling between pairs of nuclei. This Hamiltonian corresponds to the weak coupling limit, where we assume that the chemical shifts between coupled spins are much greater than their respective couplings, i.e. $|v_i^L - v_j^L| >> J_{ij}/2$. If this approximation is not valid, we need to use the full coupling Hamiltonian $\sigma_x^i\sigma_x^j + \sigma_y^i\sigma_y^j + \sigma_z^i\sigma_z^j$ in place of $\sigma_z^i\sigma_z^j$. The exact values of the Hamiltonian parameters are determined by fitting experimental data.

Single-spin control

For quantum information processing, we need to be able to perform arbitrary manipulations of a single spin, which is equivalent to arbitrary rotations about any axis. As an example, consider the application of a magnetic field $\vec{B}_1$ perpendicular to the z axis which oscillates at the nuclear spin's Larmor frequency:

$$\vec{B}_1 = |\vec{B}_1|\left(\cos(\omega^{rf}t)\vec{x} + \sin(\omega^{rf}t)\vec{y}\right) \tag{2}$$

where $\omega^{rf} = 2\pi v^{rf}$ is the angular frequency of the field. In the rotating frame of the nucleus (i.e. the frame rotating at the same frequency as the spin), $\vec{B}_1$ will appear as a constant field pointing along its rotating x axis. The spin will start to precess about this axis. Rotation about any axis in the xy-plane is possible by adjusting the phase of the $\vec{B}_1$ field, e.g. $\omega^L t \rightarrow \omega^L t + \phi$, which will create a rotation around the axis making an angle ϕ with the x axis. In the laboratory, such a rotating field can be applied by sending a radio-frequency (RF) pulse of a particular duration and phase to a conducting coil surrounding the sample, calculated according to the rotating wave approximation (see [4] for more details).

To better understand this phenomenon from the viewpoint of quantum mechanics, consider the rotating frame picture: suppose the spin is in the state $|\psi(t)\rangle$, and define the state in the rotating frame of the pulse with angular frequency ω^{rf} as

$$|\psi\rangle_r = R_z(-\omega^{rf}t)|\psi(t)\rangle \tag{3}$$

$$= R_z(-\omega^{rf}t)e^{-\frac{i}{\hbar}H_{nat}t}|\psi(0)\rangle$$

$$= e^{\frac{i}{2}\sigma_z\frac{\omega_z^{rf}}{2}t}e^{-\frac{i}{\hbar}H_{nat}t}|\psi(0)\rangle$$

$$= |\psi(0)\rangle, \text{ for a single spin with } \omega^{rf} = \omega^L. \tag{4}$$

If we apply a time derivative to equation 3, it can be shown that the state in the rotating frame $|\psi\rangle_r$ evolves according to the

Schrödinger equation with the new Hamiltonian

$$H_r = R_z(-\omega^{rf}t)H_{nat}R_z(\omega^{rf}t) - \frac{\omega^{rf}}{2}\sigma_z.$$ (5)

When an RF pulse with phase ϕ is applied to the spin, the laboratory frame Hamiltonian is:

$$H = \frac{\omega^L}{2}\sigma_z + \frac{\omega^{nut}}{2}\left(\cos(\omega^{rf}t+\phi)\sigma_x + \sin(\omega^{rf}t+\phi)\sigma_y\right)$$ (6)

where $\omega^{nut} = \pi\gamma_i|\vec{B_1}|$. In the rotating frame this becomes

$$H_r = \frac{1}{2}(\omega^L - \omega^{rf})\sigma_z + \frac{1}{2}\omega^{nut}(\cos\phi\,\sigma_x + \sin\phi\,\sigma_y).$$ (7)

Thus, if the RF pulse is at the same frequency as the spin, the spin will see a constant field in the xy plane, and will precess about it. The rotation angle θ is determined by the interval τ during which the RF field is applied, according to $\theta = \omega^{nut}\tau$.

Adding a second spin

It is also possible to independently control two spins with different Larmor frequencies. Applying an RF pulse at the frequency of the first spin, the rotating frame Hamiltonian is given by

$$\widetilde{H}_{nat} = \frac{1}{2}\omega_1^{nut}\sigma_x^1 + \frac{1}{2}\omega_2^{nut}\sigma_x^2 + \frac{1}{2}(\omega_2^L - \omega_1^L)\sigma_z^2 + \frac{\pi}{2}J_{12}\sigma_z^1\sigma_z^2$$ (8)

where we have set $\phi = 0$ for simplicity. While the first spin undergoes a rotation around the x axis, the second spin experiences a field with an additional non-zero z component. This is called the off resonance effect. If we consider the case where $\omega_2^L - \omega_2^L \gg \omega_1^{nut}$ then the second spin rotation around the x axis will average to zero during the time the first spin has completed its rotation. Typically, ω^{nut} is smaller than 1 MHz, so this condition is automatically satisfied if the two nuclei belong to different species. If the spins are of the same species, this condition can also be satisfied if a very low amplitude pulse is used due to the small nutation frequency. In this case, one drawback is that the pulse will necessarily take much longer to achieve the same angle of rotation, and if the two spins have a significant coupling constant J_{12} coupling effects might introduce significant errors and therefore limit our control.

Fortunately, there exist well known techniques to address different nuclei of the same species with high precision. The most common technique is to control the spins using shaped pulses. The frequency response to the pulse will depend on the pulse shape (Fourier theorem) and so by applying the pulse with a time varying power we can control the power spectrum of the pulse. For example, if a Gaussian shaped pulse is applied at frequency ω^{rf}, then only spins within a Gaussian distribution of frequencies around ω^{rf} will respond to this RF field. Therefore, if the height and the length of the Gaussian pulse is carefully chosen, one spin can be "addressed", causing negligible effects to others. This technique permits control of spin pairs with smaller chemical shift differences in shorter periods of time, hence allowing stronger coupling. The length of a Gaussian

pulse is proportional to the inverse of the chemical shift between the spins. Therefore, in the limiting case of small chemical shift differences and large J-coupling values, control of the qubits is more difficult.

For most liquid state experiments on a few spins, where chemical shifts are comparatively large and J-couplings are small, the use of Gaussian pulses is sufficient to achieve very high precision spin rotations. The situation becomes more complicated when there are more homonuclear spins (implying smaller chemical shift differences on average), or stronger coupling like in solid state or liquid crystal environments. It is still possible to overcome these drawbacks by considering more complicated pulse shapes and phase modulation. For example, in the section on Optimal Control for Strongly Coupled Spin, we will describe how it is possible to find shaped pulses that can implement any desired evolution by simulating the full quantum dynamics.

The controlled-NOT operation

In the previous subsection we discussed a method used to independently control different spins. In order to perform quantum computing, we need to achieve universal control and hence be able to have spins interact with each other. A two-qubit gate that is useful for quantum information processing is the controlled-NOT, which acts as

$$|00\rangle \rightarrow |00\rangle, |10\rangle \rightarrow |11\rangle$$ (9)
$$|01\rangle \rightarrow |01\rangle, |11\rangle \rightarrow |10\rangle.$$

The operation must flip the target qubit (second bit) if and only if the first qubit is in the state $|1\rangle$. In NMR, $|0\rangle$ and $|1\rangle$ are associated with the state of the spin pointing up, $|\uparrow\rangle$ or pointing down $|\downarrow\rangle$ respectively. If we look at the Hamiltonian in equation (1), and consider its effect on spin 2 depending on whether the state of spin 1 is up or down, we obtain an effective Hamiltonian for the second spin:

$$H_\uparrow^2 = \frac{1}{2}(\omega_2^L + \pi J_{12})\sigma_z^2$$ (10)

$$H_\downarrow^2 = \frac{1}{2}(\omega_2^L - \pi J_{12})\sigma_z^2.$$ (11)

Therefore, spin 2 will rotate slower or faster depending on the state of spin 1. If the coupling evolves for a time $\tau = \frac{1}{2J_{12}}$, we obtain a controlled-Z rotation of $\frac{\pi}{2}$ degrees, which can be transformed into a controlled-NOT by a few single spin pulses applied before and after (see Figure 1 for the complete sequence to implement a controlled-NOT).

In the previous sections, we demonstrated that it is possible to implement any rotation around an arbitrary axis in the xy-plane, as well as perform a controlled-NOT gate with two spins. These two conditions are sufficient to perform universal quantum computing. For practical purposes, it is convenient to use only $\frac{\pi}{2}$ and π RF pulses as they are easier to calibrate. Arbitrary angle rotations can still be applied because z-axis rotations can
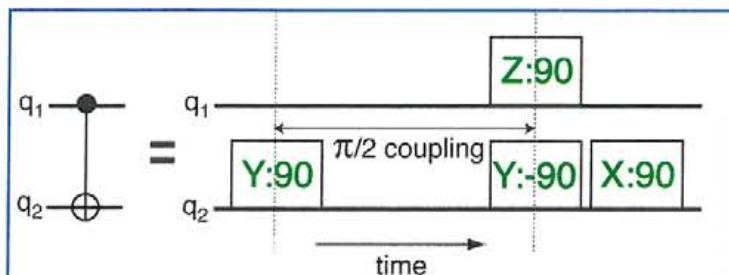
Fig. 1 Implementation of a controlled-NOT gate in liquid state NMR. The left circuit is the quantum circuit representation of a controlled-NOT gate with control qubit q_1 and target qubit q_2. On the right is the NMR implementation of such a gate by combining single qubit rotations and the natural two spin interaction of the system. The single qubit rotation properties are given in the rectangles, e.g. X:90 is a short notation for $R_x(\frac{\pi}{2}) = e^{-i\frac{\pi}{4}\sigma_x}$. Notice that the size of the rectangles are not to scale for liquid state NMR, where the RF pulses are usually much shorter than the time to implement a $\frac{\pi}{2}$ J-coupling.
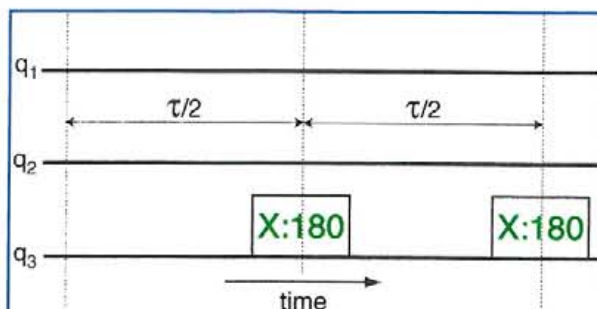

Fig. 2 In NMR, the coupling between spins is always active. It is possible to refocus 2-qubit interactions using special pulse sequences. An example is given above, where halfway through a period τ, a π pulse on one of the nuclei is implemented that reverses the direction of its spin. Note that when we have a coupling of the form $\sigma_z^1 \sigma_z^2$ the effect of the pulse can be thought of as reversing the sign of the coupling, and thus allows to cancel the interaction that occurred during the first $\tau/2$ period. This pulse sequence effectively decouples the third qubit from the system, while leaving the coupling between $q1$ and $q2$ unchanged. This situation is mathematically treated in equation (12).

be obtained by changing the definition of the rotating frame, which is equivalent to changing the phase of subsequent pulses. It can be verified that

$$R_x(\frac{\pi}{2})R_z(\theta) = R_z(\theta)R_n(\frac{\pi}{2}) \qquad (12)$$

where the vector $\vec{n} = \cos\theta\vec{x} - \sin\theta\vec{y}$. Therefore, since z rotations commute with the internal Hamiltonian of the system, we may commute all the z rotations to the end of the pulse sequence and compensate for any remaining rotation during the post-processing of the data. Moreover, the overall z-rotation takes no time and is far more precise when using this procedure because the RF phase has a higher accuracy than the RF amplitude in modern NMR spectrometers.

Refocusing and control techniques

In an NMR system, spins constantly couple to each other, and we must "turn off" these couplings on demand to implement generic quantum gates. For example, consider a three spin system in which we wish to implement a controlled-NOT between the first and second qubits. As mentioned above, a $\frac{\pi}{2}$ J-coupling between spins 1 and 2 is needed, which is accomplished by allowing the system to evolve under the natural Hamiltonian for a time $\tau = \frac{1}{2J_{12}}$. During this time spin 3 will also couple to spins 1 and 2, giving an unwanted evolution. However, if we apply a π pulse on the third spin half-way through the free evolution (at time $\frac{\tau}{2}$), this spin will effectively decouple from the other two spins and, upon an extra π pulse at the end of the evolution (at time τ), it will be returned to its initial state (this pulse sequence is shown in Figure 2). Considering only the interaction term of the intramolecular component of the Hamiltonian, we can write the evolution of the system as:

$$U(t) = R_x^{\dagger 3}(\pi)e^{-iH\tau/2}R_x^3(\pi)e^{-iH\tau/2}$$
$$= (i\sigma_x^3)e^{-i\frac{\pi\tau}{4}(J_{12}\sigma_z^1\sigma_z^2 + J_{13}\sigma_z^1\sigma_z^3 + J_{23}\sigma_z^2\sigma_z^3)}(-i\sigma_x^3)e^{-i\frac{\pi\tau}{4}(J_{12}\sigma_z^1\sigma_z^2 + J_{13}\sigma_z^1\sigma_z^3 + J_{23}\sigma_z^2\sigma_z^3)}$$
$$= e^{-i\frac{\pi\tau}{4}(J_{12}\sigma_z^1\sigma_z^2 - J_{13}\sigma_z^1\sigma_z^3 - J_{23}\sigma_z^2\sigma_z^3)}e^{-i\frac{\pi\tau}{4}(J_{12}\sigma_z^1\sigma_z^2 + J_{13}\sigma_z^1\sigma_z^3 + J_{23}\sigma_z^2\sigma_z^3)}$$
$$= e^{-i\frac{\pi\tau}{2}J_{12}\sigma_z^1\sigma_z^2}, \qquad (13)$$

where $R_x^3(\pi)$ is the operator of a π-pulse about the x-axis on spin 3. This is called a refocusing scheme and can be readily generalized to any number of coupled spins, i.e. a π pulse on spin i will effectively decouple it from all the other spins. This scheme can also be efficiently generalized to decouple m spins from each other and from the $N-m$ remaining spins. In practice, the situation is more complex. For example, one must keep track of the Zeeman evolution of all the spins (which is called phase tracking). This evolution can be taken into account by changing the phase of subsequent pulses according to the relation given in equation 12.

For systems involving up to a few spins, pulse phases and decoupling sequences are derived by hand, but for molecules containing greater number of spins, these calculations become tedious and computer assisted techniques are used [5]. Efficient classical algorithms can be implemented that optimize pulse sequences with respect to phase and residual coupling errors.

A major source of pulse errors are off resonance and coupling errors. It is possible to estimate and compensate for these errors by evaluating the first-order coupling and phase errors generated by a pulse. This is done by assuming that the real pulse can be decomposed as the ideal pulse preceded and followed by phase and coupling errors (see Figure 3). Since the error terms all commute with each other, they can be estimated using pairwise spin simulations, which requires reasonable computational resources, i.e. is efficient as we scale the number of nuclei. With small J-couplings and short pulses it is reasonable to expect error rates below a fraction of a percent for each pulse.

Once the errors generated by each pulse are known they can be taken into account and corrected for by optimizing the dura-
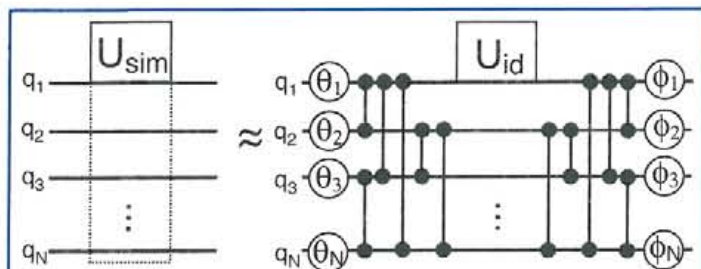
Fig. 3   A selective pulse designed to implement a single-qubit rotation in an *N*-spin system will, in general, also affect the other spins. This can be studied in small systems by simulating the full quantum dynamics to obtain the unitary U_{sim}. The unwanted evolution of the non-target qubits is represented by the broken line on the left figure. If the pulse is carefully designed so that its implementation is very close to the ideal desired unitary U_{id}, the error can be efficiently estimated to first order by phase errors (represented by θ_i and ϕ_i) and coupling errors occurring before and after the pulse.

tions of the free evolution periods and the timing of the refocusing pulses. Such an algorithm can also perform phase tracking and modify the pulse phases accordingly. Very high gate fidelities have been demonstrated using this efficient pairwise simulation technique.

Optimal control for strongly coupled spins

In some cases, spins are so strongly coupled that the approximation of $\sigma_z^i \sigma_z^j$ couplings used above breaks down. In those cases another technique can be used: strongly modulating pulses designed using numerical optimal control techniques [6,7]. For systems containing about less than ten qubits, we can find extremely high fidelity and robust control by applying optimal control principles. Just as classical optimal control theory can tell how to best steer a rocket, quantum optimal control gives the tools to best steer a quantum system to a desired unitary gate. Quantum optimal control has been used for some time in the context of driving chemical reactions with shaped laser pulses [8]. There, the goal is to maximize the transfer from a known initial state to a known final state. In the context of quantum computing, we do not necessarily know what the input state will be, and so we must find unitary gates which will work correctly for any input state.

The Hamiltonian at any point in time can be written down as

$$\mathcal{H}_{tot}(t) = \mathcal{H}_{nat} + \mathcal{H}_{rf}(t), \qquad (14)$$

where, $\mathcal{H}_{nat}$ is the time-independent, natural (or drift) Hamiltonian, and $\mathcal{H}_{rf}(t)$ represents the controllable time-dependent RF fields which we can use to drive the evolution of the system. The task is to find the sequence of control fields that will produce the correct unitary evolution. For reasonably complicated systems analytical solutions are beyond reach; however, using a numerical search we can find control sequences with fidelities as high as 0.999999. The control fields are discretized at a suitable rate (see Figure 4) and a ran-

dom guess for the control sequence is chosen. We can simulate the evolution of the system under this sequence and obtain the simulated unitary U_{sim}. We can then compare this to our goal unitary U_{goal} through a fitness function,

$$\Phi = \left| Tr\left(U_{sim}^\dagger U_{goal} \right) / 2^n \right|^2 \qquad (15)$$

which is equivalent to the state overlap fidelity averaged over all input states [6]. We can then use any optimization routine to search for the highest Φ.

The first step in this direction for NMR quantum information processing was the scheme of Fortunato *et al.* [6] who, by limiting the form of the control fields to a small number of constant amplitude, phase and frequency periods, were able to find high fidelity control sequences through a simplex search. Many more control periods can be considered and the numerical search substantially sped up through the use of standard optimal control techniques to obtain information about the gradient of the fitness function at each point.

This is the GRadient Ascent Pulse Engineering or GRAPE algorithm introduced by Khaneja *et al.* [7]. From the simulation information we can calculate approximate gradients of the fitness function with respect to the control amplitude at each timestep (see Figure 4). With this gradient information we can update the control fields by moving along the steepest ascent direction and then repeat the procedure. Convergence to a global maximum is of course not guaranteed as this hill climbing algorithm is a local search. However, empirically we find we can achieve sufficiently high fidelities from such local maxima. Convergence of the algorithm can be further improved by using non-linear conjugate gradients [9].

The control sequences drive the system through a complicated and non-intuitive path and small errors in our modeling of the system's Hamiltonian might lead to a low fidelity pulse. Fortunately, the control sequences can also be made robust against static inhomogeneities or uncertainties such as field inhomogenties and amplitude miscalibration of pulses.
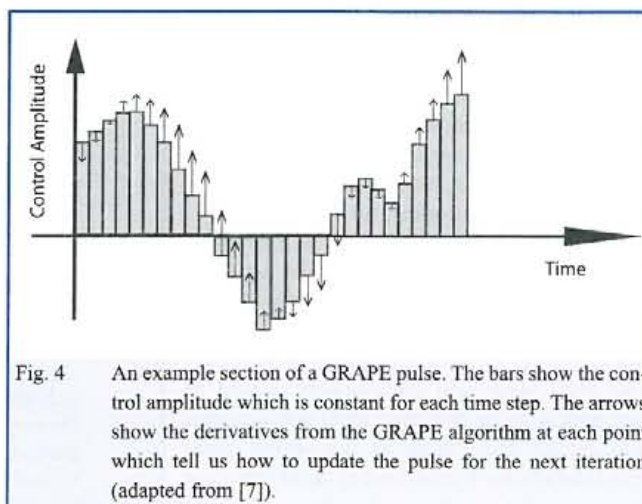

Fig. 4   An example section of a GRAPE pulse. The bars show the control amplitude which is constant for each time step. The arrows show the derivatives from the GRAPE algorithm at each point which tell us how to update the pulse for the next iteration (adapted from [7]).

Robustness to both these effects for a particular pulse is shown in Figure 6b.

Recent work on a 12-qubit liquid state system that compared this method with the more traditional approach outlined in previous sections can be found in [10]. Not surprisingly, the control using strongly modulating pulses was more precise but at an exponential cost in searching for the pulse sequences.

The scheme described above can be generalized if we can break the molecule into strongly coupled subsystems which are themselves weakly coupled, and thus it is possible to perform the decomposition described in previous sections between subsystems using pairwise simulation of subsystems. Gates to implement rotations within the subsystem will however require numerical optimization methods such as GRAPE. The details of this hybrid method are presently under investigation.

The ability to control liquid state nuclear spin systems has allowed implementation of a variety of benchmarking experiments and algorithms on small qubit registers. For example, we have developed sufficient control to implement quantum error correcting protocols [11-15], the simulation of quantum systems [16-20] and the benchmark 12 qubit quantum processor [10]. An extensive list of these and other experiments can be found at http://arxiv.org/.

SOLID STATE NMR

Solid state NMR presents a very different spin environment in comparison to liquid state NMR. Dipolar couplings do not average to zero in solids and in fact tend to dominate the NMR spectra, usually through significant broadening of the resonance peaks. As an illustration, consider an array of identical spins on a crystalline lattice: any one nuclear spin couples most strongly to its nearest neighbors, then to next-nearest neighbors, and so on (the dipolar coupling is long range, falling off as r^{-3} where r is the distance between spins). At low spin polarizations, each coupling induces a splitting of the spin's resonance energy into two components of slightly higher and lower energies. Averaging over the ensemble of spins, a smoothly broadened resonance is observed, whose width is comparable to the size of the nearest-neighbor coupling. These couplings can be quite large compared to the J-couplings observed in liquids; for example, a proton pair separated by 2Å has a maximal dipolar coupling frequency of 15 kHz, whereas proton-proton J-couplings are usually 200 Hz or less.

The solid state spin environment would at first appear to be less than ideal for quantum information processing, as the strong spin-spin interactions would lead to rapid effective

loss of coherent quantum information. However, this situation can be remedied in two ways: (1) the evolution due to time-independent interactions is, in principle, completely refocusable by appropriate RF pulse sequences and (2) the spatial dilution of spins in the sample can be used to minimize spin-spin interactions. For the three-qubit processor described in the next sub-section based on the malonic acid single crystal, we take advantage of both spin dilution and NMR refocusing techniques to maintain good qubit coherence. Additionally, spin-lattice relaxation times T_1 can be very long (minutes to hours) in solids, particularly for spin-1/2 nuclei in crystalline solids at low temperatures and with low impurity or defect densities. We generally have $T_1 > T_2 >> T_2^*$, where T_2^* is the dephasing time in the absence of refocusing, and T_2 is the "intrinsic" coherence time which is usually determined in practice for solid state systems by the quality of the refocusing controls. With perfect control, we should obtain $T_2 = 2T_1$, which would allow for many thousands of quantum gates to be performed within the characteristic coherence time scale. Of course, in practice, control errors and other experimental imperfections greatly limit the effective spin coherence time.

Besides the potential for much longer coherence times, solid state NMR also offers the prospect of greatly increasing spin polarization by cooling the sample to low temperatures. Nuclear Zeeman energies at attainable magnetic fields are, however, on the order of 1 μeV or less, and such small energies require a temperature less than 10 mK to reach full polarization by thermal equilibrium. Fortunately, nuclei may also be polarized dynamically at much more accessible temperatures ~1.5K, by driving polarization exchange between nuclear spins and a small concentration of unpaired electrons that have been introduced into the sample [21]. Since the magnetic
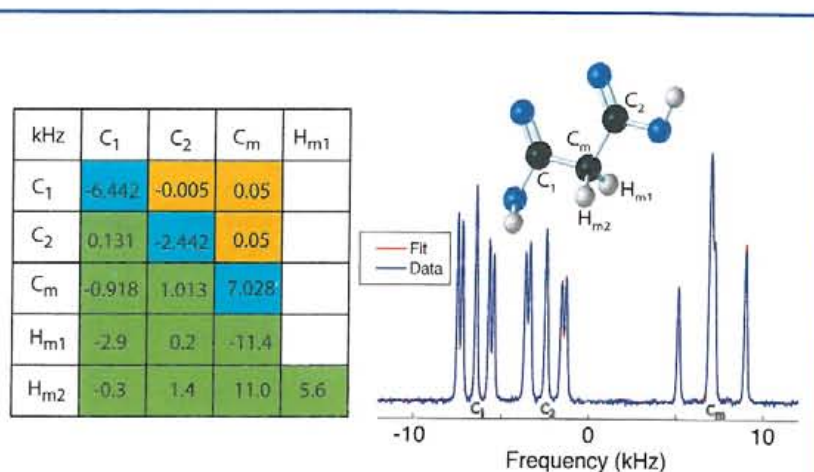

kHz	C_1	C_2	C_m	H_{m1}
C_1	-6.442	-0.005	0.05	
C_2	0.131	-2.442	0.05	
C_m	-0.918	1.013	7.028	
H_{m1}	-2.9	0.2	-11.4	
H_{m2}	-0.3	1.4	11.0	5.6

Fig. 5 (right) Fitted spectrum of a malonic acid single crystal (3.5% $^{13}C_3H_4O_4$ concentration) at a particular orientation with respect to the external field. (left) Table showing the Hamiltonian parameters extracted from the spectral fitting: chemical shifts are along the diagonal, dipolar couplings in the lower off-diagonal (green), and J-couplings in the upper off-diagonal (yellow). The dipolar parameters involving the methylene proton $H_{m1,2}$ spins have been estimated indirectly by using the ^{13}C parameters to precisely determine the crystal orientation, and knowledge of the crystal structure from neutron scattering data [28] to then calculate the couplings.
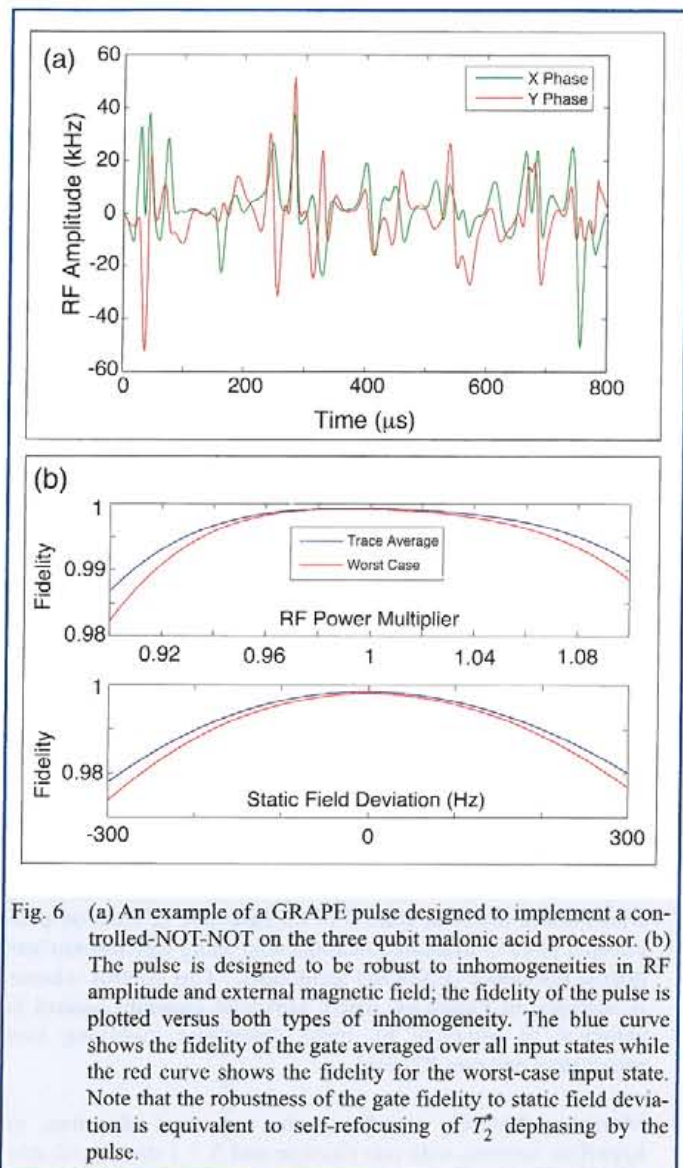
Fig. 6 (a) An example of a GRAPE pulse designed to implement a controlled-NOT-NOT on the three qubit malonic acid processor. (b) The pulse is designed to be robust to inhomogeneities in RF amplitude and external magnetic field; the fidelity of the pulse is plotted versus both types of inhomogeneity. The blue curve shows the fidelity of the gate averaged over all input states while the red curve shows the fidelity for the worst-case input state. Note that the robustness of the gate fidelity to static field deviation is equivalent to self-refocusing of T_2^* dephasing by the pulse.

moment of the electron is about 660 times larger than that of the proton, electron spins can be fully polarized in thermal equilibrium at such temperatures.

More generally, nuclear and electron spins incorporated into a solid lattice are thought to be promising elements for building scalable quantum information processors [22-24]. Nanofabrication technologies are continually growing in precision and sophistication, allowing ever more controllable nanoscale devices. Nuclear spins can provide stable qubit storage, and the transfer of information to electron spins can allow for fast operations and coupling to optical photons can provide initialization, readout and long-range entanglement [23-26]. Controlling the nuclear and electron spins with high fidelity using magnetic resonance should play an important role in these schemes.

Three qubit solid state quantum information processor

The following example of a small quantum information processor is based on malonic acid, $C_3H_4O_4$ [29]. The sample is a single crystal (grown from aqueous solution) consisting of a mixture of $^{12}C_3H_4O_4$ and $^{13}C_3H_4O_4$ (labeled) molecules; ^{13}C is spin-1/2 whereas ^{12}C is spinless. The fraction of labeled molecules is kept to < 10% of the total, so that the $^{13}C_3$ molecules can function as an ensemble of 3-qubit registers with relatively weak spin interactions between registers. It is important to note that all molecules contain 4 spin-1/2 ^1H atoms, so that generally, a decoupling RF sequence must be applied to the spins to isolate the ^{13}C qubits from the ^1H spin system. Figure 5 shows a ^{13}C NMR spectrum (with ^1H decoupling) obtained at an external field magnitude and orientation at which the three carbons are well separated in Larmor frequency (i.e. separately addressable) and the carbon-carbon intramolecular dipolar couplings are relatively large, allowing for fast coupling gates. The spin Hamiltonian of the 3-qubit system is determined directly by fitting a simulated spectrum to the measured one. The height differences between the absorption peaks are due to the "strong coupling" effect, in which non-diagonal terms in the coupling Hamiltonian (such as d_{12} $(\sigma_x^1\sigma_x^2 + \sigma_y^1\sigma_y^2)$) have frequencies d_{12} comparable to the difference in chemical shifts of the coupled spins $\Delta\omega^L$.

When $d_{12} \sim \Delta\omega^L$ as in the present solid state system, the σ_z^i eigenstates (i.e. the computational basis states $|000\rangle$, $|001\rangle$, etc.), are no longer the energy eigenstates and the spin dynamics become more complex. This poses a challenge for universal quantum control: the scalable method described in the section on Refocusing and Control Techniques for generating quantum gate pulse sequences in liquid state NMR is valid only when such mixing is negligible. However, numerically optimized strongly modulating pulses can succeed in providing sufficient control.

This control can be made robust with respect to sources of ensemble incoherence. For example, the linewidths $((T_2^*)^{-1})$ of the resonance peaks visible in Figure 5 are about two orders of magnitude larger than those seen in a liquid environment. This incoherence is mainly due to a combination of residual dipolar couplings between $^{13}C_3H_4O_4$ molecules and inhomogeneity of the external magnetic field over the sample [39]. Strongly modulating pulses can be made sufficiently robust to these effects with minimal added computational overhead, particularly when using the GRAPE algorithm (see Figure 6).

Algorithmic Cooling

As a computational demonstration of the malonic acid quantum processor, we now consider the experimental implementation of a heat-bath algorithmic cooling (HBAC) protocol [31]. The aim of the experiment is to amplify the polarization on one of the three qubits, using both qubit-qubit operations and a controlled coupling to a surrounding "heat-bath" [32,33]. Note that HBAC is a classical algorithm, since each step results in a classical state of the system, however we use quantum gates in its implementation. Strongly modulating pulses obtained using
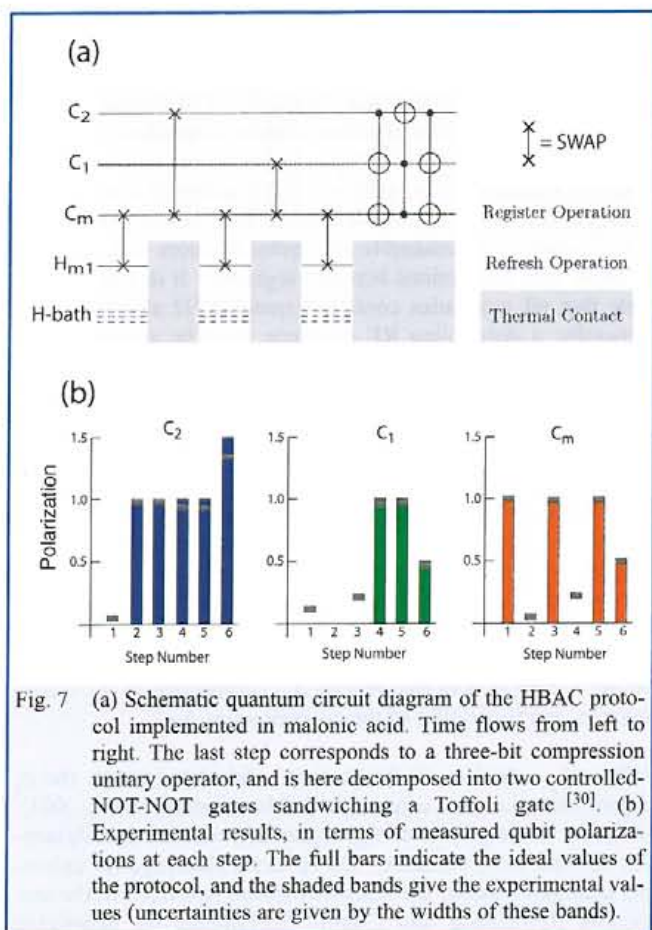
Fig. 7 (a) Schematic quantum circuit diagram of the HBAC proto-col implemented in malonic acid. Time flows from left to right. The last step corresponds to a three-bit compression unitary operator, and is here decomposed into two controlled-NOT-NOT gates sandwiching a Toffoli gate [30]. (b) Experimental results, in terms of measured qubit polariza-tions at each step. The full bars indicate the ideal values of the protocol, and the shaded bands give the experimental val-ues (uncertainties are given by the widths of these bands).

GRAPE are used to perform gate operations on the qubits. The HBAC algorithm operates on the three malonic acid qubits as well as the large surrounding ^1H spin system which acts as a spin-bath with a large effective heat capacity. Figure 7a shows a schematic quantum circuit diagram of the first six steps of the HBAC protocol implemented in the malonic acid system. The swap operations between C_m and H_{m1} (labeled 'refresh' in Figure 7a) can be carried out either using a dual $^{13}C/^1H$ multi-ple-pulse refocusing sequence [31,34] or by using Hartmann-Hahn cross-polarization [35] with short contact time [40].

The multi-qubit operations are carried out using strongly mod-ulating pulses. During these operations, a strong continuous wave decoupling field is applied to the ^1H spins, serving both to decouple them from the carbons and to "lock" their collec-tive magnetization along a particular direction in the rotating frame (the latter is called 'spin-locking' and is used to prevent the magnetization from dephasing). This continuous wave field permits the protons to interact with each other via the $^1H - ^1H$ dipolar couplings. Such couplings diffuse spin polar-ization [36] through the Hamiltonian terms of the form $\sigma_+^1\sigma_-^2 + \sigma_-^1\sigma_+^2$ [41]. Therefore, the H_{m1} polarization of the spins restore to the equilibrium value of the ^1H bath after sufficient interaction time. The timescale for such equilibration in this system is $\sim 50 \times T_2^*(H) \approx 5ms << T_1(H)$.

Experiments were performed at room temperature in the regime of low nuclear spin polarization, and the aim was to demonstrate quantum control similar to what has been achieved using liquid state NMR quantum information proces-sors. The measured polarizations on each of the qubit spins at each step of the algorithm are shown in Figure 7. The full bars indicate ideal values and the shaded bands give the experimen-tal values. A rough indication of the fidelity of the experimen-tal protocol can be gauged by the ratio of the final polarization of the target qubit C_2 to its ideal value, $F \approx 1.39/1.5 = 92.7\%$. This yields an average error (here loss of polarization) per step of about 1.5%. Given that the inhomogeneous line-broadening effects (i.e. the natural incoherence of the system) in solid state NMR is two orders of magnitude larger than that in liquid state, this is an impressive degree of control. Furthermore, these results indicate that such sequences applied to single quantum systems would yield much higher fidelities. We are presently implementing a multiple-round HBAC algorithm with the goal of moving beyond the 1.5 signal amplification benchmark that uses only unitary transformation.

CONTROL OF COUPLED ELECTRON-NUCLEAR SYSTEMS

An attractive direction for spin-based quantum information processing is to couple the nuclear spin degree of freedom with that of the electron spin. The larger magnetic moment of the electron leads to a much faster timescale for spin manipulation, and the electron's charge degree of freedom can serve as a pathway for initialization and readout of spin qubits. Early progress in this direction was made by Mehring et al. [37,38], who showed coherent control of an ensemble of electron-pro-ton spin pairs in irradiated malonic acid using electron-nuclear double resonance (ENDOR) techniques. This control scheme is sketched in Figure 8a, where universal quantum control is achieved in principle by pulse sequences involving two microwave and one RF field.

Moreover, Mehring introduced the important idea that, in hyperfine systems with one electron and $N > 1$ distinguishable nuclear spins, quantum gates operating on nuclear states could be sped up significantly using the hyperfine interaction with the electron to mediate indirect nuclear-nuclear interac-tions [24]. This was dubbed the S-bus concept since the elec-tron spin operator is often denoted as S. The S-bus concept is suggestive of a picture in which isolated clusters of 1 elec-tron + N nuclear spins form qubit sub-registers, where a hand-ful of qubits can be manipulated and stored with high fidelity.

Initialization of the electron spins to the ground state $|0\rangle$ occurs thermally at modestly low temperatures and typical external magnetic fields. The nuclear spin qubits can be initialized one by one by alternating polarization swaps with the electron spin and waiting for subsequent electron thermalization $(T_1^{elec} << T_1^{nuc})$. There are various possibilities for coupling sub-registers: the electron-electron exchange coupling modu-lated by electrostatic gates [22], direct dipolar coupling between electrons, or long-range coupling using optical tech-
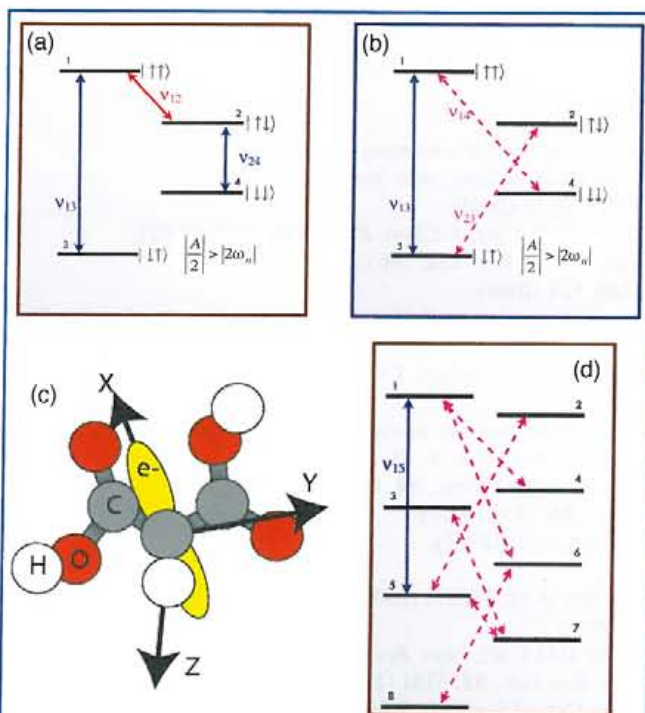
Fig. 8 (a) The ENDOR model for universal quantum control of an electron-nuclear hyperfine coupled spin pair. All states can be reached using three control parameters: two electron transitions at microwave frequencies (blue arrows) and one nuclear transition at radio-frequency (red arrow). (b) If the system has an anisotropic hyperfine interaction, universal control can be achieved using only one microwave control field. The mixing of states connected by "forbidden" transitions (dashed arrows) occurs under the hyperfine interaction, allowing pathways to all states. Modulated sequences of the single control field can be found using the GRAPE method to generate arbitrary unitary gates. (c) Stable radical of malonic acid, produced by x-ray irradiation. One of the methylene protons is removed by irradiation, leaving behind an unpaired π-electron spin-1/2. The maximum hyperfine couplings to the methylene ^{13}C and ^{1}H are 220 and 90 MHz, respectively. (d) A representative level connectivity diagram for a 1e-2n system in an orientation for which the anisotropic hyperfine terms are large. Universal quantum control is achievable by implementing appropriate modulated sequences on the microwave transition labeled v_{15}. A ^{13}C labeled nucleus on the methylene carbon of malonic acid would exhibit a similar level structure.

niques [23,25-27]. A recent proposal outlines a method to further improve the computational power of the S-bus concept. This proposed method uses the natural anisotropy of the hyperfine interaction to "mix" spin sublevels (much as the strong coupling effect discussed above mixes nuclear spin computational basis states). This eliminates the need for direct RF control of the nuclear spin transitions. This method is shown schematically in Figure 8b. The effective spin Hamiltonian of the electron-nuclear pair has the form:

$$H_{en} = \omega_e^L S_z + \omega_n^L I_z + A_z S_z I_z + A_x S_z I_x, \qquad (16)$$

where A_x (A_z) is the anisotropic (isoptropic) hyperfine coupling, **S** and **I** are the electron and nuclear spin operators, and ω_e^L and ω_n^L are the Larmor frequencies. If we arrange the system such that $A_x \sim \omega_n^L$, there will be efficient mixing of the sublevels indicated by the dashed arrows in Figure 8b, due to the hyperfine term $A_x S_z I_x$.

It can be shown mathematically that controlled driving of a single microwave transition (indicated as the 1-3 transition in Figure 8b) is enough to generate any unitary operator when given sufficient bandwidth, duration and complexity of the control field. This remarkable result allows for much faster operations by replacing the low energy nuclear excitation field with the higher energy hyperfine coupling. It also simplifies the experimental setup by requiring only one control frequency. Moreover, we can apply optimal control pulse-shaping methods such as GRAPE to generate universal quantum gates. Experimental work is currently underway with the aim of demonstrating these techniques using hyperfine coupled spin systems such as the stable malonic acid radical (see Figure 8c-d).

CONCLUSION

Of the many proposed and current realizations of quantum information processing devices, NMR stands out as the present leader in terms of control fidelities and the manipulation of the largest number of quantum bits. This has allowed for the implementation of a variety of benchmarks and algorithms that bring theoretical concepts to the laboratory. Its success is built on many years of RF engineering invested in NMR technology for a variety of purposes that have recently been adapted for quantum information processing. Combining such control with the long coherence times of nuclear spins makes NMR promising for quantum computation.

One of the present difficulties with using only nuclear spins is the ability to initialize them into pure states. Therefore the next generation of magnetic resonance based devices will make use of electron spins both to initialize nuclear spin qubits and to mediate interactions between them, yielding much faster gate operations. We expect this research to continue to produce exciting results and to merge with other quantum technologies in the coming years.

ACKNOWLEDGEMENTS

REFERENCES

1. E.M. Purcell, H.C. Torrey, and R.V. Pound, *Phys. Rev.*, **69**, 37 (1946).
2. F. Bloch, *Phys. Rev.*, **70**, 460 (1946).
3. P. Kaye, R. Laflamme, and M. Mosca, *An introduction to quantum computing*, Oxford University Press (2007).
4. M.H. Levitt, *Spin dynamics: Basics of nuclear magnetic resonance*, John Wiley & Sons, New-York (2001).
5. M.D. Bowdrey, J.A. Jones, E. Knill, and R. Laflamme, *Phys. Rev. A*, **72**, 032315 (2005).
6. E.M. Fortunato, M.A. Pravia, N. Boulant, G. Teklemariam, T.F. Havel, and D.G. Cory, *J. Chem. Phys.*, **116**, 7599 (2002).
7. N. Khaneja, T. Reiss, C. Kehlet, T. Schulte-Herbruggen, and S.J. Glaser, *J. Mag. Res.*, **172**, 296 (2005).
8. H. Rabitz, R. de Vivie-Riedle, M. Motzkus, and K. Kompa, *Science*, **288**, 824 (2000).
9. A.E. Bryson and Y.C. Ho, *Applied optimal control: optimization, estimation, and control*, Hemisphere Pub. Corp. Washington DC, (1975).
10. C. Negrevergne, T.S. Mahesh, C.A. Ryan, M.J. Ditty, F. Cyr-Racine, W. Power, N. Boulant, T.F. Havel, D.G. Cory, and R. Laflamme, *Phys. Rev. Lett.*, **96**, 17501 (2006).
11. D.G. Cory, M.D. Price, W. Maas, E. Knill, R. Laflamme, W.H. Zurek, T.F. Havel, and S.S. Somaroo, *Phys. Rev. Lett.*, **81**, 2152 (1998).
12. M. Laforest, D. Simon, J.C. Boileau, J. Baugh, M.J. Ditty, and R. Laflamme, *Phys. Rev. A*, **75**, 012331 (2007).
13. D.G. Cory, S.S. Somaroo, T.F. Havel, E. Knill, R. Laflamme, and W.H. Zurek, *Mol. Phys.*, **98**, 1347 (2000).
14. E. Knill, R. Laflamme, R. Martinez, and C. Negrevergne, *Phys. Rev. Lett.*, **86**, 5811 (2001).
15. N. Boulant, L. Viola, E.M. Fortunato, and D.G. Cory, *Phys. Rev. Lett.*, **94**, 130501 (2005).
16. Z. Chen, J. Yepez, and D.G. Cory, *Phys. Rev. A* **74**, 042321 (2006).
17. C. Negrevergne, R. Somma, G. Ortiz, E. Knill, and R. Laflamme, *Phys. Rev. A* **71**, 032344 (2005).
18. T.F. Havel, Y. Sharf, L. Viola, and D.G. Cory, *Phys. Rev. A*, **280**, 282 (2001).
19. C.H. Tseng, S. Somaroo, Y. Sharf, E. Knill, R. Laflamme, T.F. Havel, and D.G. Cory, *Phys. Rev. A*. **61**, 012302 (2000).
20. S. Somaroo, C.H. Tseng, T.F. Havel, R. Laflamme, and D.G. Cory, *Phys. Rev. Lett.*, **82**, 5381 (1999).
21. A. Abragam and M. Goldman, *Nuclear Magnetism: Order and Disorder*, Oxford Scientific Publishers, New York, (1982).
22. B.E. Kane, *Nature*, **393**, 133 (1998).
23. L. Jiang, J.M. Taylor, A.S. Sorenson, and M.D. Lukin, *Scalable Quantum Networks based on Few-Qubit Registers*, (2007), quant-ph/0703029.
24. M. Mehring and J. Mende, *Phys. Rev. A*, **73**, 052303 (2006).
25. F. Jelezko, T. Gaebel, I. Popa, A. Gruber, and J. Wrachtrup, *Phys. Rev. Lett.*, **92**, 076401 (2004).
26. F. Jelezko, T. Gaebel, I. Popa, M. Domhan, A. Gruber, and J. Wrachtrup, *Phys. Rev. Lett.*, **93**, 130501 (2004).
27. L. Childress, M.V. Gurudev Dutt, J.M. Taylor, A.S. Zibrov, F. Jelezko, J. Wrachtrup, P.R. Hemmer, and M.D. Lukin, *Science*, **314**, 281 (2006).
28. R.C. McCalley and A.L. Kwiram, *J. Phys. Chem.*, **97**, 2888 (1993).
29. J. Baugh, O. Moussa, C.A. Ryan, R. Laflamme, C. Ramanathan, T.F. Havel, and D.G. Cory, *Phys. Rev. A*, **73**, 022305 (2006).
30. T. Toffoli, in *Automata, Languages and Programming*, edited by W. de Bakker and J. van Leeuwen, Springer, New York, (1980), p. 632, technical Memo MIT/LCS/TM-151, MIT Lab. for *Comput. Sci.* (unpublished).
31. J. Baugh, O. Moussa, C.A. Ryan, A. Nayak, and R. Laflamme, *Nature*, **438**, 470 (2005).
32. L. Schulman, T. Mor, and Y. Weinstein, *Phys. Rev. Lett.*, **94**, 120501 (2005).
33. P.O. Boykin, T. Mor, V. Roychowdhury, F. Vatan, and R. Vrijen, *Proc. Natl. Acad. Sci. USA*, **99**, 3388 (2002).
34. D.P. Weitekamp, J.R. Garbow, and A. Pines, *J. Chem. Phys.*, 77, 2870 (1982).
35. S.R. Hartmann and E.L. Hahn, *Phys. Rev.*, **128**, 2042 (1962).
36. W. Zhang and D.G. Cory, *Phys. Rev. Lett.*, **80**, 1324 (1998).
37. M. Mehring, J. Mende, and W. Scherer, *Phys. Rev. Lett.*, **90**, 153001 (2003).
38. M. Mehring, W. Scherer, and A. Weidinger, *Phys. Rev. Lett.*, **93**, 206603 (2004).
39. This inhomogeneity is mainly caused by susceptibility mismatch between the crystal and the air/glass surrounding it, and the fact that it is non-spherical.
40. The former approximates a universal quantum swap operation, whereas the latter is sufficient for swapping polarization.
41. These terms involve the ladder operators defined as $\sigma_\pm = \sigma_x \pm i\sigma_y$.